AIP Journal of Applied Physics

Tensile testing of Fe and FeCr nanowires using molecular dynamics simulations

J. Byggmästar, F. Granberg, A. Kuronen, K. Nordlund, and K. O. E. Henriksson

Citation: Journal of Applied Physics **117**, 014313 (2015); doi: 10.1063/1.4905314
View online: http://dx.doi.org/10.1063/1.4905314
View Table of Contents: http://scitation.aip.org/content/aip/journal/jap/117/1?ver=pdfcov
Published by the AIP Publishing

Tensile testing of Fe and FeCr nanowires using molecular dynamics simulations

J. Byggmästar,[a] F. Granberg, A. Kuronen, K. Nordlund, and K. O. E. Henriksson
Department of Physics, University of Helsinki, P.O. Box 43, Helsinki FIN-00014, Finland

(Received 13 November 2014; accepted 19 December 2014; published online 7 January 2015)

Using molecular dynamics, we have studied the behaviour of cylindrical [001]-oriented Fe and FeCr nanowires under uniaxial tensile strain with both an embedded atom method (EAM) and a Tersoff-like bond order potential. The mechanical properties were analysed and the deformation mechanism was studied and compared between the potentials. The effects of chromium content and size of the wire were studied. Both potentials show elongation by deformation twinning in the $\langle 111\rangle/\{211\}$ system resulting in a significantly stiffer and stronger [110]-axial nanowire. The pure iron nanowires are elastically softer than bulk iron and an addition of chromium has both a softening and weakening effect. The bond order potential shows a strong dependence on chromium concentration, while the dependence is considerably weaker for the EAM potential. © *2015 AIP Publishing LLC*. [http://dx.doi.org/10.1063/1.4905314]

I. INTRODUCTION

Mechanical properties of nanowires are of interest from both a fundamental and a practical point of view. Examining the behaviour and properties of nanostructures enables testing of the fundamental elastic and plastic properties of metallic single crystals[1,2] and other materials[3–5] on the atomic level. In the development of micro- and nanoelectromechanical systems (MEMS, NEMS), the mechanical properties need to be well known in order to attain reliability and stability of the system.

Due to the difficulty of carrying out experiments on the nanoscale, molecular dynamics (MD) simulations play an important role in studying the properties of nanowires. Tensile test simulations provide insight into the behaviour of the nanowire, such as strength, elasticity, ductility, and deformation mechanism. For the latter, there are mainly two competing mechanisms; twinning and slip. In some cases, the nanowire may also be deformed through a solid-solid phase transition. Slip causes irreversible plastic deformation as opposed to twinning, which can lead to a so-called pseudoelastic behaviour where the initial shape of the nanowire is recovered through a reverse twinning mechanism. If the temperature is low, heating the twinned nanowire up to a critical temperature can spontaneously initiate the reverse twinning motion, leading to a shape memory effect in the nanowire.[6–8] It is widely understood that this reverse twinning mechanism is driven by a minimisation of surface energy, providing the compressive force needed to recover the initial shape.[6–12] Pseudoelasticity and the closely connected shape memory effect in nanowires have been extensively studied in fcc metals[6–10] for their potential use in a variety of applications such as sensors and actuators in NEMS.[13,14]

A similar pseudoelastic behaviour has also been observed in bcc Fe nanowires.[11,12] It was found that the initial [100]/{011} nanowire, where [100] denotes the axial direction and {011} the surfaces, transforms into a [011]-oriented wire by a 90° rotation of the unit cell during twinning. A compressive strain results in detwinning back to the initial state. Other studies on Fe nanowires have investigated the solid-solid phase transitions induced by axial strain for a range of temperatures,[15] diameters,[16] and crystal orientations.[17] It was observed that bcc Fe nanowires can transform into close-packed structures at a critical strain.

In this study, we focus on cylindrical Fe and FeCr nanowires with Cr concentrations between 0 and 20 at. %. We investigate their behaviour under uniaxial tensile strain using both an embedded atom method (EAM) and a Tersoff-like bond order potential (BOP). We summarise the elastic and plastic properties and show that twinning is always the preferred deformation mechanism over slip, regardless of potential and Cr concentration. Pseudoelasticity is studied by applying a compressive strain on the reoriented nanowire. Furthermore, we observe an indication of a reconstruction into an ultrathin pentagonal structure before fracture. Finally, we review the differences between the results obtained with the two potentials.

II. SIMULATION AND ANALYSIS METHODS

All simulations were performed using the classical molecular dynamics code PARCAS.[18,28,29] The simulations were carried out with two interatomic potentials, a Tersoff-like BOP by Henriksson *et al.*[19] and the two-band EAM potential by Olsson *et al.*[20]

We studied cylindrical nanowires with diameters of 2, 4, and 6 nm in the BOP and 2 and 4 nm in the EAM potential. Five different Cr concentrations, 0, 5, 10, 15, and 20 at. %, were simulated. For each Cr concentration and diameter, three separate cases were simulated to get an insight into the stochasticity of the deformation. Additionally, for pure Fe nanowires, diameters in the range of 2–12 nm were simulated

[a]Electronic mail: jesper.byggmastar@helsinki.fi

to get the size dependence of the Young's modulus. All simulations were performed at 300 K.

The cylindrical nanowires were constructed from a {100} bcc block using the appropriate lattice parameter for each potential at 300 K. The block was cut to the desired radius with the crystal orientation [001] in the axial direction. For the FeCr nanowires, substitutional Cr atoms were randomly inserted in the block to get the desired concentrations. For each case, a new block was constructed to get a unique wire with different randomly positioned Cr atoms. The length of the wire L was chosen as $L = 4D$, where D is the diameter. The wires were initially relaxed for 20 ps at 300 K using a Berendsen-type temperature control.[21] All nanowires retained their initial shape throughout the relaxation period. The nanowires were subjected to a constant axial strain rate of $\dot{\varepsilon} = 10^{-6}\,\mathrm{fs}^{-1}$. Test runs with slower strain rates yielded identical results. The strain rate is computed relative to the initial simulation box length and is implemented by rescaling all atom coordinates at each time step. Periodic boundary conditions were applied in the axial direction to model an infinitely long wire, while the surface was kept free.

The stress-strain relations were obtained from the simulations and analysed. Fig. 1 shows a typical stress-strain curve with the computed quantities marked. The Young's modulus, E_{001}, was obtained by calculating the slope in the $\varepsilon = [0, 0.03]$ interval, in which the stress-strain relation was clearly linear for all cases. The upper yield strength, σ_{UYS}, is the maximum stress in the elastic region, the ultimate tensile stress, σ_{UTS}, is the overall maximum stress as shown in Fig. 1, and the fracture strain, ε_{frac}, is the strain at which the wire breaks. The Poisson's ratio, ν_{001}, was determined by first repeatedly computing an average radius R of the wire using the outermost shell of atoms for strain states in the interval $\varepsilon = [0, 0.03]$, then calculating the slope of the obtained $(\Delta L/L_0, -\Delta R/R_0)$ data, where L_0 is the initial length and R_0 the initial radius.

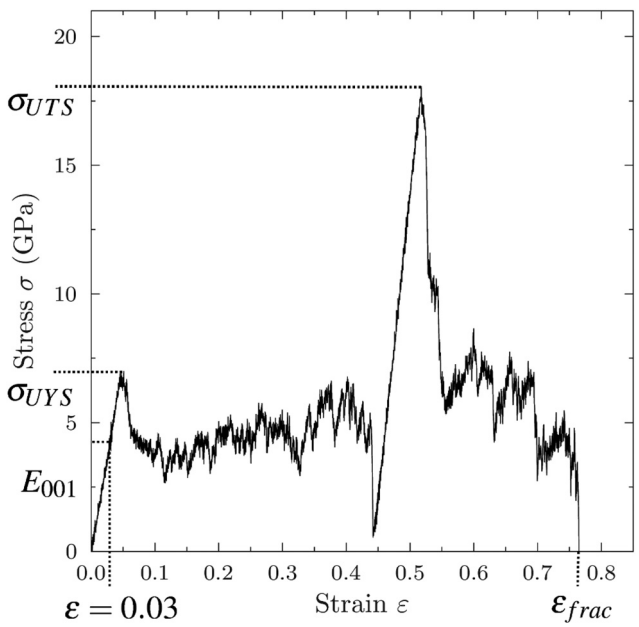

FIG. 1. A typical stress-strain curve illustrating the analysed quantities.

III. RESULTS AND DISCUSSION

A. Mechanical properties

The numerical results of the mechanical properties are given in Tables I and II for both interatomic potentials. The tables show that the Young's modulus, upper yield strength, and Poisson's ratio vary only a little from case to case, while the ultimate tensile strength and fracture strain have a big variation. This is because the latter two are dependent on the plastic deformation of each case, as discussed in Sec. III B.

TABLE I. The numerical results with the BOP. The unit of the Young's modulus, upper yield strength, and ultimate tensile strength is GPa. The Cr concentrations are given in at. %.

	D (nm)	Case	E_{001}	ν_{001}	$\sigma_{UY\,S}$	σ_{UTS}	ε_{frac}
Fe	2	1	178.2	0.328	11.9	34.2	1.00
		2	175.9	0.332	12.4	34.0	0.80
		3	176.4	0.335	12.0	33.6	0.91
	4	1	202.9	0.341	9.8	28.8	0.84
		2	202.5	0.343	9.9	24.4	1.10
		3	203.5	0.341	9.8	18.9	1.00
	6	1	213.7	0.347	9.1	16.4	0.98
		2	214.0	0.343	9.0	28.2	1.04
		3	213.5	0.340	9.1	13.1	0.95
FeCr(5%)	2	1	140.9	0.370	6.9	18.1	0.76
		2	145.6	0.366	8.0	18.8	0.75
		3	138.7	0.369	7.2	18.4	0.85
	4	1	152.3	0.378	6.0	17.5	0.86
		2	151.8	0.375	6.0	15.4	1.02
		3	152.6	0.376	5.8	17.5	0.83
	6	1	154.9	0.377	5.5	13.6	0.93
		2	153.9	0.377	5.7	17.5	1.04
		3	155.2	0.369	5.6	10.6	0.85
FeCr(10%)	2	1	117.3	0.385	5.7	15.2	0.78
		2	117.7	0.394	5.8	12.1	0.79
		3	122.4	0.398	6.1	12.5	0.78
	4	1	120.6	0.403	4.3	13.1	0.81
		2	118.8	0.396	4.4	10.4	0.75
		3	121.2	0.403	4.5	13.3	1.05
	6	1	117.5	0.397	4.0	13.6	0.99
		2	116.5	0.390	4.0	12.6	1.10
		3	117.2	0.388	4.1	12.1	0.87
FeCr(15%)	2	1	98.6	0.426	4.7	12.5	0.70
		2	91.1	0.462	5.4	13.2	0.76
		3	97.8	0.418	5.0	12.0	0.70
	4	1	97.6	0.400	3.7	11.5	0.78
		2	98.0	0.403	3.7	10.8	0.92
		3	98.8	0.424	3.7	11.9	0.84
	6	1	95.3	0.409	3.3	11.4	0.84
		2	92.5	0.411	3.2	10.7	0.84
		3	94.7	0.407	3.3	10.3	0.78
FeCr(20%)	2	1	83.8	0.462	4.9	8.7	0.68
		2	85.7	0.448	4.9	10.4	0.68
		3	98.6	0.428	4.7	9.2	0.83
	4	1	86.8	0.410	3.2	9.9	0.76
		2	87.1	0.423	3.2	10.2	0.76
		3	82.0	0.414	3.2	9.7	0.89
	6	1	80.2	0.415	2.8	9.4	0.71
		2	81.0	0.423	2.8	9.3	0.73
		3	79.4	0.423	2.8	9.6	0.88

TABLE II. The numerical results with the EAM potential. The unit of the Young's modulus, upper yield strength, and ultimate tensile strength is GPa. The Cr concentrations are given in at. %.

	D (nm)	Case	E_{001}	ν_{001}	$\sigma_{UY\,S}$	σ_{UTS}	ε_{frac}
Fe	2	1	123.0	0.373	11.1	29.5	0.91
		2	123.5	0.371	10.7	23.5	0.97
		3	124.9	0.368	10.9	19.7	1.15
	4	1	135.1	0.369	10.3	10.4	0.81
		2	134.7	0.371	10.3	14.4	1.28
		3	134.5	0.368	10.4	10.9	1.06
FeCr(5%)	2	1	118.0	0.374	9.7	23.4	0.96
		2	117.8	0.379	9.9	27.1	1.12
		3	118.1	0.372	10.0	19.4	1.06
	4	1	126.7	0.372	9.2	14.3	1.29
		2	127.0	0.368	9.1	9.3	0.65
		3	126.5	0.369	9.2	17.1	1.27
FeCr(10%)	2	1	115.3	0.374	9.2	19.1	1.09
		2	114.7	0.372	9.3	24.3	1.00
		3	114.6	0.368	8.8	9.2	0.94
	4	1	121.8	0.368	8.4	9.7	0.92
		2	122.1	0.372	8.4	8.5	0.70
		3	121.5	0.376	8.5	14.6	1.32
FeCr(15%)	2	1	112.6	0.372	8.5	15.2	0.88
		2	112.0	0.369	8.5	19.1	1.01
		3	113.1	0.371	8.4	16.8	0.86
	4	1	118.8	0.365	7.8	7.9	0.96
		2	118.1	0.362	7.6	16.6	1.36
		3	118.0	0.367	7.9	9.6	1.14
FeCr(20%)	2	1	111.3	0.374	8.3	18.3	0.99
		2	111.1	0.373	7.7	17.3	0.98
		3	111.2	0.367	7.9	8.0	0.61
	4	1	114.5	0.378	7.3	21.1	1.13
		2	115.2	0.375	7.4	13.6	0.98
		3	114.5	0.369	7.3	15.7	1.13

Fig. 2 shows the size dependence of the Young's modulus for pure Fe. The Young's moduli are normalised by the obtained bulk values at 300 K, 142.3 GPa for the EAM potential and 225.6 GPa for the BOP. Thin Fe nanowires are softer than bulk Fe, and the Young's modulus approaches the bulk value non-linearly as the diameter grows. This is understandable, as the fraction of surface atoms decreases non-linearly with increasing diameter and is only a few percent for 10 nm and bigger nanowires. The experimental value for the Poisson's ratio for bulk iron[22] is 0.368 at 300 K, and the simulated values 0.359 and 0.357 for the EAM and BOP, respectively. As seen in Tables I and II, the values for Fe nanowires are close to their bulk counterparts with the BOP values being a few percent lower and the EAM a few percent higher than the bulk values. Tables I and II clearly show that the upper yield strength is highest for thin Fe nanowires and drops as the diameter is increased. This is also true for the ultimate tensile strength, although it varies strongly from case to case, as discussed in Sec. III B. The nanowires show high ductility with fracture strains of around 1.0 and above.

Fig. 3 illustrates the Cr dependence on the Young's modulus with Cr concentrations of 0–20 at. %. It is clear that addition of Cr has a softening effect on the nanowires, the Young's modulus drops when more substitutional Cr atoms are added. The difference in elasticity between the two diameters presented is also more distinct for pure Fe compared to higher Cr concentrations. The BOP shows a much more drastic Cr dependence on the Young's modulus and all other quantities, but as seen in Tables I and II the general trend is that Cr has both a softening and weakening effect. Both the upper yield strength and ultimate tensile strength decreases with increasing Cr concentration. The Poisson's ratio remains fairly stable regardless of diameter and Cr concentration for the EAM potential, while the value has a clear Cr dependence in the BOP. This is also true for the fracture strain; the nanowires become less ductile with the BOP, while no evident change can be seen in the EAM results.

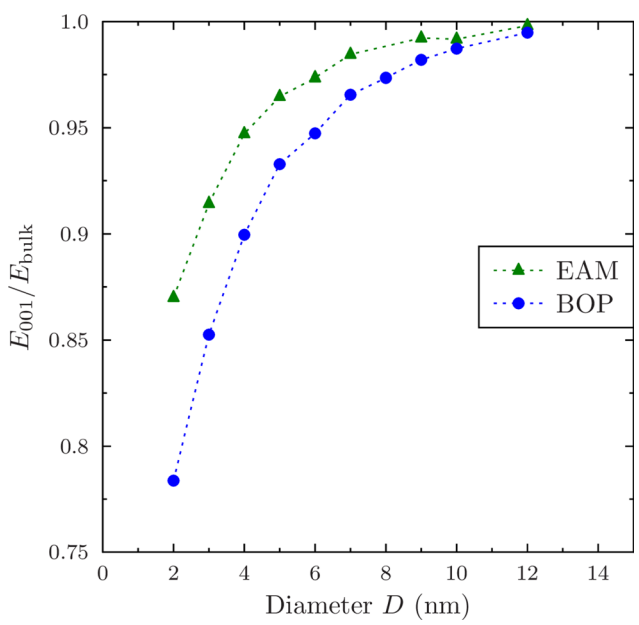

FIG. 2. The diameter dependence on the Young's modulus for pure Fe.

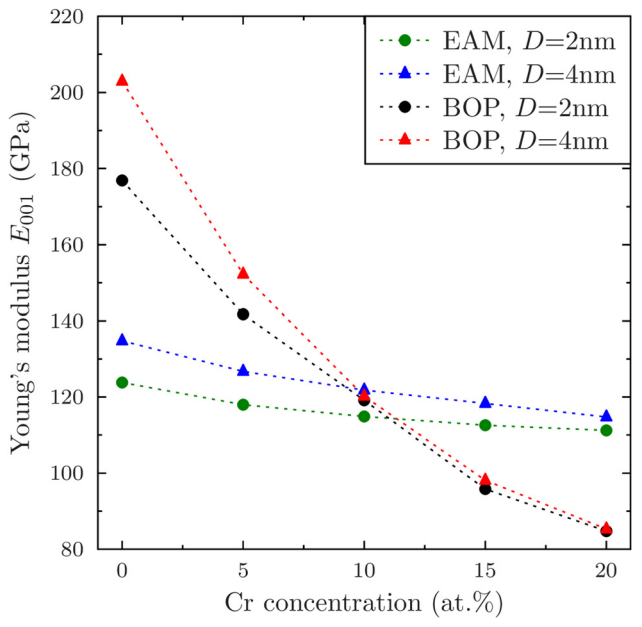

FIG. 3. Young's modulus of the 2 and 4 nm nanowires at each Cr concentration.

B. Deformation twinning and pseudoelastic behaviour

Fig. 4 shows the stress-strain relation during deformation of the 2 nm Fe nanowire using the BOP (case 1). The wire is first elastically strained up to the yield point (11.9 GPa), at which the stress drops drastically. The wire is then easily elongated at slowly rising stress levels in the range of 2–6 GPa through twinning, as described in more detail below. At a strain of about 45%, the twin boundary has propagated through the whole length and the nanowire, that is now back in a single-crystalline configuration, is again elastically strained up until the second yield point, which gives the ultimate tensile strength at 34.2 GPa. Necking occurs at the second yield point and finally fracture at a strain of 1.00.

Fig. 5 illustrates the nucleation of the twin boundary in a 2 nm Fe nanowire in detail. An initial ⟨111⟩/{211} stacking fault is formed and atoms in adjacent {211} planes start moving in the ⟨111⟩ direction, forming the twin region. As the wire is strained, the twin region is allowed to grow layer by layer through partial dislocation slip in the ⟨111⟩/{211} system. The lattice unit cell is rotated 90° relative to the longitudinal axis over the twin boundary, resulting in a change of axial direction from [001] to [110]. The highlighted atoms in Fig. 5 illustrate the movement of atoms that leads to the change in orientation. This deformation mechanism has previously been studied in detail for square-shaped bcc nanowires.[11] If the twin boundaries are allowed to propagate perfectly across the whole length, they annihilate each other and the result is a complete, thinner [110]-axial nanowire with a more elliptic cross section. This reoriented wire has a significantly higher Young's modulus and strength as visible in the stress-strain curve in Fig. 4.

The perfect [001] → [110] reorientation was observed for all 2 nm cases in the BOP. For the EAM potential, after the initial formation of the twin boundary the atoms in the twinned region were unable to reorganise perfectly, leaving a rough surface on the reoriented nanowire. For the 4 nm cases in the EAM potential, necking occurred before the twin boundaries were allowed to propagate through the whole length, while complete reorientation was seen in the majority of the cases in the BOP. This provides an explanation for the large differences in ultimate tensile strength (σ_{UTS}) seen in Tables I and II.

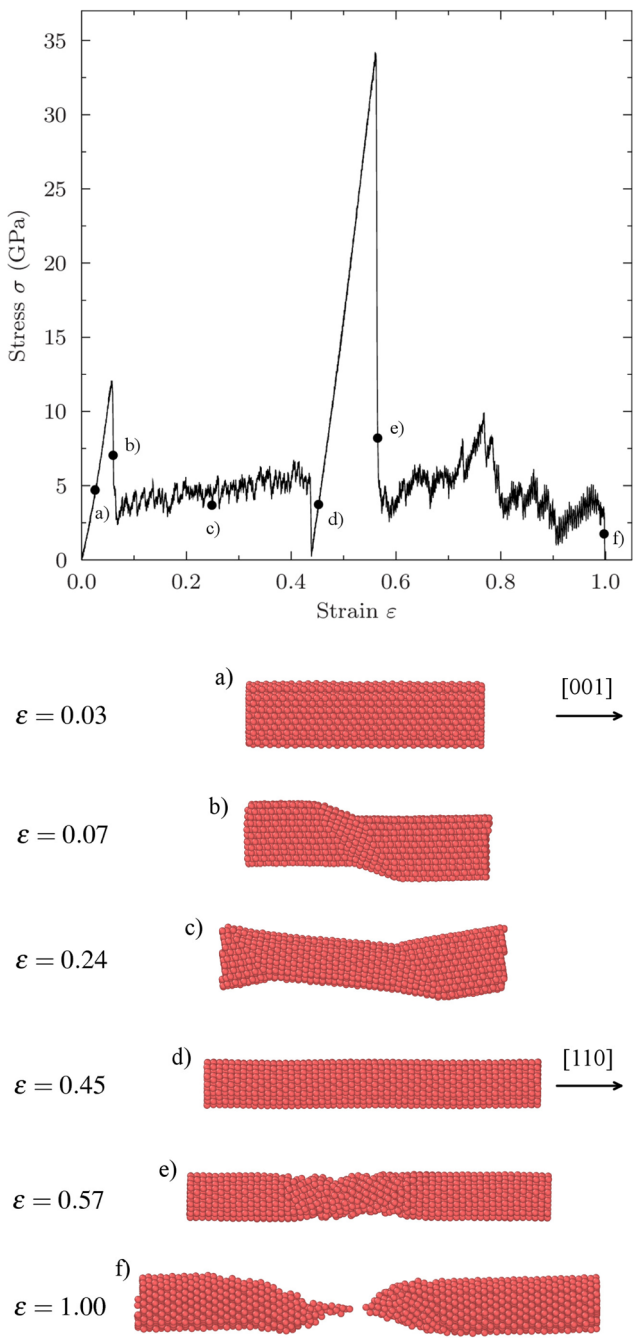

FIG. 4. (Top) Stress-strain curve of the 2 nm Fe nanowire in the BOP (case 1) and (bottom) side view snapshots of the different stages of deformation.

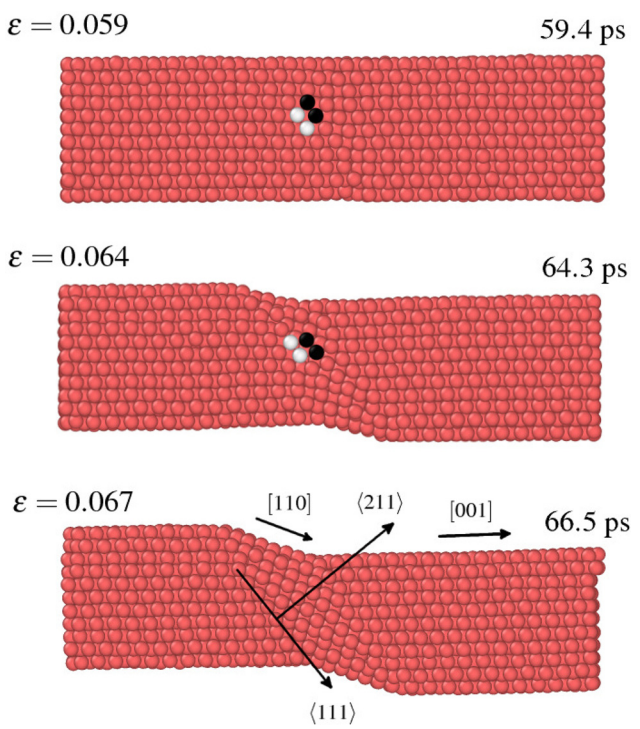

FIG. 5. Side view snapshots of the cylindrical 2 nm Fe nanowire during the formation of the twin boundary.

The reversibility of the twinning mechanism has previously been studied for square-shaped bcc nanowires.[11,12] To investigate this for cylindrical nanowires, a negative strain rate was applied to the reoriented wire at $\varepsilon \approx 0.45$. The [110] nanowire transformed back to the [001] wire through a reverse twinning deformation, showing that pseudoelastic behaviour can also occur in cylindrical Fe nanowires in addition to the previously studied square-shaped nanowires with well-defined surfaces.

Twinning was also the only deformation mechanism in the FeCr nanowires. Although the Cr atoms noticeably interfered with the propagation of the twin boundary, complete reorientation was seen for all Cr concentrations. The Cr atoms also made a smooth reorganisation more difficult, resulting in the reoriented [110] FeCr nanowires being more roughly structured, as opposed to the almost perfectly structured wire for pure Fe as seen in Figs. 4 and 6. This caused necking to occur at lower strains and also lowered the overall strength of the wires. Perfect pseudoelasticity was therefore not expected. Some simulations using a compressive strain were, however, carried out with the BOP to study the reverse twinning and the state of the detwinned wire as compared to the initial nanowire. Full reverse twinning did occur for all Cr concentrations, but as expected the resulting detwinned [001] nanowire had a rougher surface than the original [001] wire, much like the reoriented [110] wire as seen in Fig. 6. Nevertheless, the original shape and orientation was recovered for all studied Cr concentration, indicating that also cylindrical FeCr nanowires can exhibit pseudoelastic behaviour.

C. Reconstruction before fracture

In some cases of the 2 nm Fe and FeCr nanowires, we saw a reconstruction into a pentagonal shaped structure shortly before fracture. This reconstruction occurred in the necking region and prolonged the breaking process. Fig. 7 shows an example illustrating this transition in a 2 nm FeCr(15%) nanowire with the EAM potential. Similar reconstructions have previously been observed and studied in fcc copper nanowires,[23–27] but has not previously been reported for initially bcc-structured nanowires. The pentagonal structure consists of a single atom chain surrounded by rings of five atoms as seen in Fig. 7. Further investigations are being carried out with thinner Fe and FeCr nanowires at elevated temperatures to study this reconstruction.

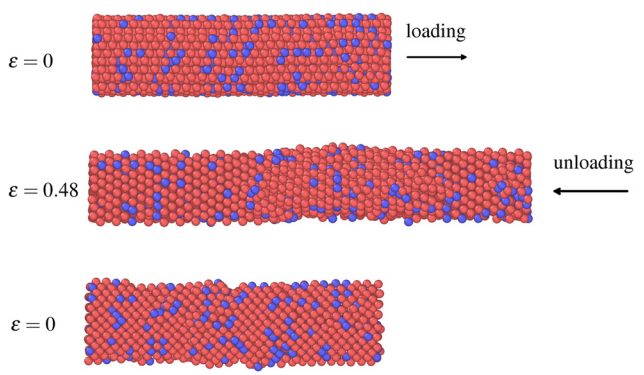

FIG. 6. The reoriented FeCr(15%) nanowire after loading and unloading in the BOP. Red: Fe, blue: Cr.

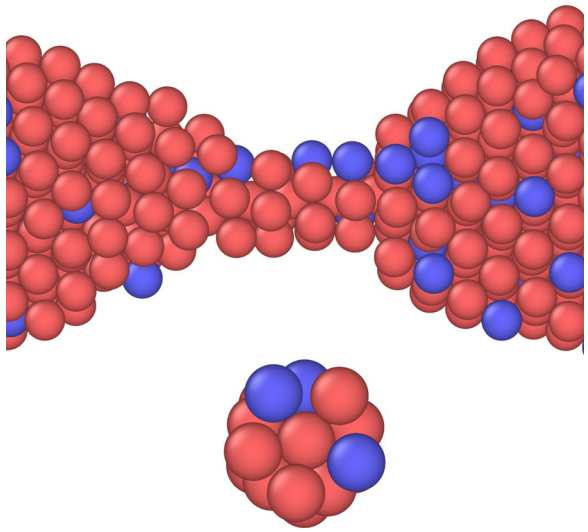

FIG. 7. (Top) Reconstruction into a pentagonal structure shortly before fracture in a 2 nm FeCr(15%) nanowire for the EAM potential and (bottom) cross section of the reconstructed section of the nanowire. Red: Fe, blue: Cr.

D. Dependence on interatomic potential

The trends of the mechanical properties are in agreement between the two potentials, the Young's modulus drops as the Cr concentration is increased, as seen in Fig. 3. The change in Young's modulus as a function of wire diameter follows a similar trend, as illustrated in Fig. 2. However, the numerical values and the effects of adding Cr atoms differ noticeably between the potentials. To examine the reasons behind this, we made test runs with an artificial version of the BOP where the Fe-Cr interactions were set equal to the Fe-Fe ones. These runs showed a much weaker dependence with Cr concentration, similar to the EAM potential results. This shows that the large difference between the potentials is explained by the BOP's relatively weak Fe-Cr interaction compared to the pure Fe-Fe interaction, leading to a more rapid decrease in Young's modulus and yield strength when the Cr concentration is increased and more Fe-Cr bonds are present, as visible in Fig. 3 and Tables I and II.

Twinning was the sole deformation mechanism before necking for both potentials, although necking and fracture sometimes occurred before complete reorientation for the EAM potential. With the BOP, almost perfect [001] → [110] transformation was seen for all Cr concentrations and diameters. The reversibility of the twinning deformation could therefore be well studied with the BOP.

IV. CONCLUSIONS

Using molecular dynamics and two different types of potentials, we have studied the behaviour of Fe and FeCr nanowires under axial tensile strain in the [001] direction. We conclude that cylindrical Fe and FeCr nanowires are elastically softer than the bulk counterparts and that the Young's modulus tends towards that of the bulk as the diameter grows. The yield strength is highest for thin Fe

nanowires and increasing the Cr concentration or the diameter has a weakening effect. These trends are in agreement between the potentials, however, the numerical values are noticeably different. The BOP shows a stronger Cr dependence, which can be explained by the relatively weak Fe-Cr interaction, compared to the pure Fe-Fe interaction. The fracture strain varies from case to case, but was found to generally be around 1.0, slightly lower for high Cr concentrations in the BOP. The ultimate tensile strength also varies strongly because of atom-level fluctuations, and is for the EAM potential highly dependent on the state of twinning in the wire when necking occurs. The variation of the Poisson's ratio for the EAM potential is small, while it is growing as the Cr concentration is increased for the BOP.

Twinning is the preferred deformation mechanism over full slip for both potentials at all studied Cr concentrations and diameters. The propagation of the twin boundary is clearly visible in the stress-strain response. The nanowire is first elastically strained up to a yield point, at which the initial twin boundary is formed. The wire is then easily elongated at low stress levels until the whole wire is in the twinned state and the [001] → [110] reorientation is complete. This reoriented wire is significantly stronger and stiffer than the initial [001] oriented wire. Continued axial strain results in necking and finally fracture. Some cases showed a reconstruction into an ultrathin pentagonal structure shortly before fracture. By applying a compressive strain to the reoriented [110] wire, pseudoelastic behaviour was observed for all Cr concentrations with the BOP. We therefore conclude that pseudoelasticity can be seen in cylindrical Fe and FeCr nanowires with diameters up to 6 nm and Cr concentrations up to at least 20 at. %.

ACKNOWLEDGMENTS

The molecular dynamics calculations presented in this article have been carried out in the CSC's computating environment. CSC is the Finnish IT center for science and is owned by the Ministry of Education. The research has been carried out with financial support from the Academy of Finland (project MIMOSE, Contract No. 259249).

[1]J.-Y. Kim and J. R. Greer, Acta Mater. **57**, 5245 (2009).
[2]S. H. Oh, M. Legros, D. Kiener, and G. Dehm, Nature Mater. **8**, 95 (2009).
[3]T. Yi, L. Li, and C.-J. Kim, Sens. Actuators, A **83**, 172 (2000).
[4]X. Wei, M.-S. Wang, Y. Bando, and D. Golberg, Adv. Mater. **22**, 4895 (2010).
[5]T. Namazu and S. Inoue, Fatigue Fract. Eng. Mater. Struct. **30**, 13 (2007).
[6]H. S. Park, K. Gall, and J. A. Zimmerman, Phys. Rev. Lett. **95**, 255504 (2005).
[7]W. Liang, M. Zhou, and F. Ke, Nano Lett. **5**, 2039 (2005).
[8]W. Liang and M. Zhou, Phys. Rev. B **73**, 115409 (2006).
[9]H. S. Park and C. Ji, Acta Mater. **54**, 2645 (2006).
[10]J. Diao, K. Gall, and M. L. Dunn, Phys. Rev. B **70**, 075413 (2004).
[11]S. Li, X. Ding, J. Deng, T. Lookman, J. Li, X. Ren, J. Sun, and A. Saxena, Phys. Rev. B **82**, 205435 (2010).
[12]J. Zhu and D. Shi, J. Phys. D **44**, 055404 (2011).
[13]S. Büttgenbach, S. Bütefisch, M. Leester-Schädel, and A. Wogersien, Microsyst. Technol. **7**, 165 (2001).
[14]K. Otsuka and T. Kakeshita, MRS Bull. **27**, 91 (2002).
[15]L. Sandoval and H. M. Urbassek, Nanotechnology **20**, 325704 (2009).
[16]L. Sandoval and H. M. Urbassek, Nano Lett. **9**, 2290 (2009).
[17]L. Sandoval and H. M. Urbassek, Appl. Phys. Lett. **95**, 191909 (2009).
[18]K. Nordlund, PARCAS computer code. The main principles of the molecular dynamics algorithms are presented in [Ref. 28 and 29], 2010.
[19]K. O. E. Henriksson, C. Björkas, and K. Nordlund, J. Phys.: Condens. Matter **25**, 445401 (2013).
[20]P. Olsson, J. Wallenius, C. Domain, K. Nordlund, and L. Malerba, Phys. Rev. B **72**, 214119 (2005); see also "Erratum,"*ibid.* **74**, 229906 (2006).
[21]H. J. C. Berendsen, J. P. M. Postma, W. F. van Gunsteren, A. DiNola, and J. R. Haak, J. Chem. Phys. **81**, 3684 (1984).
[22]J. J. Adams, D. S. Agosta, R. G. Leisure, and H. Ledbetter, J. Appl. Phys. **100**, 113530 (2006).
[23]J. C. González, V. Rodrigues, J. Bettini, L. G. C. Rego, A. R. Rocha, P. Z. Coura, S. O. Dantas, F. Sato, D. S. Galvão, and D. Ugarte, Phys. Rev. Lett. **93**, 126103 (2004).
[24]V. K. Sutrakar and D. R. Mahapatra, Nanotechnology **20**, 045701 (2009).
[25]J. Zhu, D. Shi, J. Zhao, and B. Wang, Nanotechnology **21**, 185703 (2010).
[26]B. Wang, J. Zhao, X. Chen, D. Shi, and G. Wang, Nanotechnology **17**, 3178 (2006).
[27]F. Granberg, S. Parviainen, F. Djurabekova, and K. Nordlund, J. Appl. Phys. **115**, 213518 (2014).
[28]K. Nordlund, M. Ghaly, R. S. Averback, M. Caturla, T. Diaz de la Rubia, and J. Tarus, Phys. Rev. B **57**, 7556–7570 (1998).
[29]M. Ghaly, K. Nordlund, and R. S. Averback, Phil. Mag. A **79**, 795 (1999).